

# Simulation of the dynamic response of transmission lines in strong winds

M. J. Matheson and J. D. Holmes

Department of Civil and Systems Engineering, James Cook University of North Queensland, Townsville, Queensland, 4811, Australia

(Received March 1980; revised October 1980)

A numerical simulation procedure for predicting the response of a single span transmission line to strong turbulent winds is described. The wind velocities are generated using a 'Monte Carlo' technique based on an inverse fast Fourier transform; the equations of motion of the line are then solved numerically using a finite difference method. Results obtained using the method were compared with those from linearized random vibration theory. Effects due to the mean swing angle of the line, and due to the excitation of an in-plane mode of vibration were apparent.

## Introduction

The loading on transmission lines and their supporting towers due to wind is an extremely important factor in their design. A more accurate knowledge of the oscillatory behaviour of transmission lines in strong winds, and of the loads transmitted to the towers, is very desirable to produce more economical designs.

The traditional design method has been based on the use of a peak gust wind speed, i.e. the largest recorded or predicted wind speed expected to occur once in a specified return period. However, it was recognized many years ago that to use the total drag force, calculated on the assumption that the design gust speed acted simultaneously along a 300–500 m span, would be extremely conservative. 'Span reduction factors' have been applied to allow for this effect. The factors presently used have often been empirically derived from the actual measurements on test lines — usually, however, at wind speeds much lower than those representative of design situations.

In recent years, a more rational approach, using random vibration theory, has been advocated by several authors.<sup>1–5</sup> In this type of analysis, which has also been applied to other structures, the reduction effect due to the lack of correlation of wind gusts along the span, and the main features of the dynamic response of the line, are taken account of in a rational manner. However, the method involves linearization both in the aerodynamics and in the line dynamic behaviour. A linear relationship between the fluctuating drag forces applied to the line and the upwind velocity fluctuations is assumed, and a linearization of the equations of motion of the line, is also made. In order to achieve the latter, it is assumed that the line tension remains constant during the motion — this assumption avoids any consideration of the extensibility of the line. These assumptions have been questioned particularly at high wind speeds.

In the present paper, a simulation procedure is described in which representative wind velocities, forces, line response and lateral tower loads are computed on a step by step

basis. In this way, all nonlinear effects are included. The simulated wind records are generated using a 'Monte Carlo' simulation procedure which recognizes the random nature of natural turbulence and allows for a realistic representation of the correlation properties of the turbulent fluctuations along the length of the span, drawing on accumulated knowledge of actual measurements of these properties in the natural wind. The method of wind record generation has been described fully by Holmes,<sup>6</sup> and has been previously applied to compute the response of a cable stayed bridge.<sup>7</sup>

A brief summary of the method of wind record generation is given in the next section. Then the partial differential equations of motion of the line and their numerical solution by finite difference methods are discussed. The interfacing of the two numerical procedures and the implementation to compute the response of a typical transmission line span is discussed, followed by some results of the computations, and a comparison is made with equivalent calculations using random vibration theory.

## Simulation of wind velocities

The basis of the numerical simulation of the wind velocity records is that the random fluctuating or turbulent component of the wind velocity at any point can be represented as a summation of cosine waves of  $N$  equally spaced frequencies, with phase angles randomly distributed between 0 and  $2\pi$  radians. The amplitude of each cosine function is chosen so that its contribution to the total mean square value is equivalent to the area under a specified target spectral density curve within a chosen frequency interval,  $\Delta n$ . In the present case the target spectrum was the von Karman-Harris wind velocity spectrum:

$$S_u(n) = \frac{1.04 \lambda_u I_u^2}{\left[ 2 + 3 \left( \frac{n \lambda_u}{\bar{u}} \right)^2 \right]^{5/6}} \quad (1)$$

where:  $\lambda_u$  is a specified wavelength in metres at which  $nS_u(n)$  is a maximum  $I_u$  is the intensity of turbulence and  $\bar{u}$  is the mean wind velocity.

A very efficient numerical procedure is obtained by using an inverse fast Fourier algorithm to carry out the summation described above. In this case, the number,  $N$ , of generated values in the simulated wind velocity sequence is equal to the number of discrete frequencies into which the specified frequency range is divided. The time increment between values,  $\Delta t$ , is equal to the reciprocal of the chosen maximum frequency.

Simulated random wind velocity records sampled along a horizontal line normal to the mean flow direction are generated by summing a number of complex number vectors before performing the inverse fast Fourier transform. Each vector is required to provide the correct correlation relationship with previously generated records.

The form of the normalized co-spectrum suggested by Davenport<sup>8</sup> is used:

$$\rho(n) = \exp \left[ -c \left( \frac{nd}{\bar{u}} \right) \right] \quad (2)$$

where  $d$  is the separation distance and  $c$  is the decay constant. For a full exposition of the simulation method, see Holmes.<sup>6</sup>

### Computation of line response

#### Partial differential equations

The mathematical equations of motion for an extensible, perfectly flexible, suspended line are presented below. These are derived by applying Newton's second law of motion to a small element of line,  $\delta s$ , as in Figure 1. The basic equation is:

$$\rho \frac{\partial^2 \mathbf{x}}{\partial t^2} = \frac{\partial}{\partial s} \left( T \frac{\partial \mathbf{x}}{\partial s} \right) + \mathbf{f} \quad (3)$$

where  $\mathbf{x}$  = displacement vector from origin;  $\rho$  = mass/length;  $t$  = time;  $s$  = curvilinear distance along line;  $T$  = tension and  $\mathbf{f}$  = force/unit length of line.

Alternatively, by establishing a reference state, denoted by a subscript '0', equation (1) can be expressed as follows:

$$\rho_0 \frac{\partial^2 \mathbf{x}}{\partial t^2} = \frac{\partial}{\partial s_0} \left( \frac{T}{(1 + \epsilon)} \frac{\partial \mathbf{x}}{\partial s_0} \right) + \mathbf{f}(1 + \epsilon) \quad (4)$$

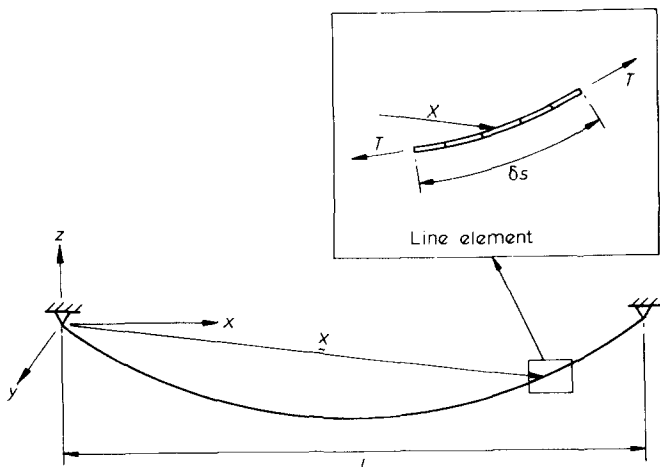


Figure 1 Suspended line and element

In this case, the reference state was taken to be the horizontal straight line between the two supports.

Where:

$\epsilon$  = strain relative to reference state

$$s = s_0(1 + \epsilon) \quad (5)$$

$$\rho = \rho_0/(1 + \epsilon) \quad (6)$$

$$\frac{\partial s}{\partial s_0} = (1 + \epsilon) \quad (7)$$

Equation (4) can be expanded into cartesian coordinates  $x, y, z$ , as follows:

$$\rho_0 \frac{\partial^2 x}{\partial t^2} = \frac{\partial}{\partial s_0} \left( \frac{T}{(1 + \epsilon)} \frac{\partial x}{\partial s_0} \right) + f_x \quad (8)$$

$$\rho_0 \frac{\partial^2 y}{\partial t^2} = \frac{\partial}{\partial s_0} \left( \frac{T}{(1 + \epsilon)} \frac{\partial y}{\partial s_0} \right) + f_y \quad (9)$$

$$\rho_0 \frac{\partial^2 z}{\partial t^2} = \frac{\partial}{\partial s_0} \left( \frac{T}{(1 + \epsilon)} \frac{\partial z}{\partial s_0} \right) + f_z \quad (10)$$

These are the three partial differential equations of motion. To provide the basis for a solution algorithm, further equations relating tension to strain and strain to displacements are necessary. The strain in an element relative to the reference state:

$$\epsilon = \frac{\delta s - \delta s_0}{\delta s_0} \quad (11)$$

by definition, and:

$$T = AE(\epsilon - \epsilon_0) + T_1 \quad (12)$$

Where:  $A$  = area of cross-section;  $E$  = modulus of elasticity;  $\epsilon_0$  = strain in an element in static state relative to reference state and  $T_1$  = tension in an element in static state.

The following assumptions have been made to implement the random vibration analysis mentioned in the introduction.<sup>3</sup>

- (a), the tension  $T$  is assumed constant throughout the cable and equal to the horizontal component under no wind loading,  $H$ .
- (b), deflections in the  $x$  and  $z$  direction are neglected.
- (c), the term  $\partial/\partial s$  is approximated by  $\partial/\partial x$ .

Hence equation (3) is reduced to:

$$\rho \frac{\partial^2 y}{\partial t^2} = H \frac{\partial^2 y}{\partial x^2} + f_y \quad (13)$$

A linear equation, like (13), can be solved by random vibration theory.

#### Numerical model

The finite difference equations are discretized versions of equations (8)–(12), given above, for a single span, fixed ended line. Two numerical algorithms have been studied, one being a direct explicit approach<sup>9</sup> and the other a semi-implicit-explicit approach.<sup>10,11</sup> The latter model allows a reduction of computation time by a factor of about ten.

Both sets of finite difference equations are very similar, and a list of those corresponding to Watts' method are presented below:

$$X_{j+1}^{n+1} = X_j^{n+1} + \{ [h(1 + \epsilon_{j+1/2}^{n+1})]^2 - [Y_{j+1}^{n+1} - Y_j^{n+1}]^2 - [Z_{j+1}^{n+1} - Z_j^{n+1}]^2 \}^{1/2} \quad (14)$$

$$\begin{aligned}
 Y_j^{n+1} = & 2Y_j^n - Y_j^{n-1} + (\Delta\tau/h)^2 \{R_{j+\frac{1}{2}}^n Y_{j+1}^n \\
 & - [R_{j+\frac{1}{2}}^n + R_{j-\frac{1}{2}}^n] Y_j^n + R_{j-\frac{1}{2}}^n Y_{j-1}^n\} \\
 & + (F_y)_j^n \Delta\tau^2 \quad (15)
 \end{aligned}$$

$$\begin{aligned}
 Z_j^{n+1} = & 2Z_j^n - Z_j^{n-1} + (\Delta\tau/h)^2 \{R_{j+\frac{1}{2}}^n Z_{j+1}^n \\
 & - [R_{j+\frac{1}{2}}^n + R_{j-\frac{1}{2}}^n] Z_j^n + R_{j-\frac{1}{2}}^n Z_{j-1}^n\} \\
 & + (F_z)_j^n \Delta\tau^2 \quad (16)
 \end{aligned}$$

$$\begin{aligned}
 R_{j+\frac{1}{2}}^{n+1} = & \{ [X_j^{n+1} - 2X_j^n + X_j^{n-1}] (h/\Delta\tau)^2 \\
 & + [X_j^{n+1} - X_{j-1}^{n+1}] R_{j-\frac{1}{2}}^n / [X_{j+1}^{n+1} - X_j^{n+1}] \} \quad (17)
 \end{aligned}$$

$$\epsilon_{j+\frac{1}{2}}^{n+1} = [(AE/T_1)(1 + \epsilon_0) - 1] / [(AE/T_1)^2 - R_{j+\frac{1}{2}}^{n+1}] - 1 \quad (18)$$

where:

$$\begin{aligned}
 l &= \text{span} \\
 X, Y, Z &= x/l, y/l, z/l \\
 F_y &= \text{dimensionless distribution wind force on an} \\
 &\quad \text{element} = f_y l / T_1 \\
 F_z &= \text{dimensionless gravitational force} = f_z l / T_1 \\
 h &= \text{dimensionless space step} = \Delta x / l \\
 \Delta\tau &= \text{dimensionless time step} = \Delta t (T_1 / \rho)^{1/2} / l \\
 R &= T / [T_1 (1 + \epsilon)] \\
 j &= \text{time } n \Delta t, \text{ node } j
 \end{aligned}$$

The method outlined by Watts<sup>10</sup> has been adopted in this study, due to its superior computational efficiency.

### Testing

To clarify any doubts about the accuracy of the finite difference algorithm, extensive tests were performed. Unfortunately, it is difficult to establish complete validity for the finite difference equations. The partial differential equations are nonlinear, and hence numerical stability cannot be proved through analytical means alone. However, by running the program and producing results for known solutions, rigorous comparisons can be made.

Tensions and displacement along a particular line when subjected to a constant load, e.g. a constant steady wind, can be compared with exact solutions. A number of such tests were undertaken and the results showed excellent agreement with the exact solutions. An indication of the performance and accuracy of the system in a dynamic situation was achieved by a free vibration analysis. Natural frequencies obtained from numerous tests were compared with those predicted analytically by Irvine and Caughey<sup>12</sup> and again showed good agreement.

Roussel<sup>9</sup> conducted a number of tests to compare the response given by his numerical model with those from measurements. The agreement was good.

Further verification of the method outlined in this paper was achieved by comparing some responses with those calculated by Roussel's method; the computed responses were essentially identical.

Table 1 Wind and line properties

Intensity of turbulence, $I_U$	0.15
Decay constant, $c$	10
Peak wavelength, $\lambda_U$	700 m
Mass density of line, $\rho$	1.69 kg/m
Line diameter, $D$	29.3 mm
Span, $l$	300 m
Horizontal tension (no wind), $H$	27.5 kN
Young's modulus, $E$	68 GPa

### Implementation

The numerical procedures described in the previous two sections were implemented to calculate the response of a particular transmission line on a DEC-10 machine. Table 1 lists the wind and transmission line properties used.

The instantaneous wind velocity, generated as described in the second on the simulation of wind velocities was converted to a result drag force per unit length using equation (19):

$$f_r(t) = \frac{1}{2} \rho_{\text{air}} C_d D u_r^2(t) \quad (19)$$

where  $u_r(t)$  is the instantaneous relative wind velocity between the air and transmission line. Thus, aerodynamic damping effects were implicitly included in the calculations. The air density  $\rho_{\text{air}}$ , was taken to be 1.20 kg/m<sup>3</sup> and the drag coefficient,  $C_d$ , was assumed to be 1.0.

The time increment for the wind simulation programme was dictated by the stability requirements of the finite difference program. Stability is ensured when:

$$\left( \frac{T}{\rho} \right)^{1/2} \frac{\Delta t}{\Delta x} < 1 \quad (\text{Watts}^{10}) \quad (20)$$

For the results described in this paper, a space step,  $\Delta x$ , of 10 m, and a time step of 0.057 s were used. Thus the transmission line span was divided into 30 elements. Wind velocities and forces were generated at 15 points along the span. This number was dictated by computing time limitations; however, an increase in the number of points where wind forces were applied, was found to produce no significant change in the response parameters. Due to limitations on computer core space, the number of generated points in the velocity and response sequences was restricted to 4096; this gave a total record length of 233 s. However, the random errors in the response calculations were minimized by ensemble averaging over a number of runs, each one using a different sequence of random numbers in the wind record generation.

### Results

Response characteristics of most interest here, are loads exerted on supports and line deflections. Time-history plots of a typical single wind record, corresponding centre span sway angle response  $\theta$ , and lateral support reaction  $R$ , are given in Figure 2.

Significant features from Figure 2 are: the sympathetic line response to the excitation force, contribution of particular frequencies to response; and the degree of fluctuations in response. The sway angle appears to be dominated by the low wind frequencies and the first sway mode frequency. However, the support reaction appears more wide band, similar to the wind velocity record and shows higher frequency components than the sway angle.

#### Mean and r.m.s. fluctuating response

Test runs using the simulation model were run for mean wind velocities ranging from 10 to 20 m/s. Mean and r.m.s. responses recorded in Table 2, represent the ensemble average of four runs at each mean wind velocity.

The r.m.s. lateral support reaction is plotted against mean wind velocity in Figure 3. Simulation points represent averaged values, while the bar-lines indicate the maximum and minimum values obtained. Comparison is made with the solution given by random vibration theory. Straight lines on this graph represent power law relationships.

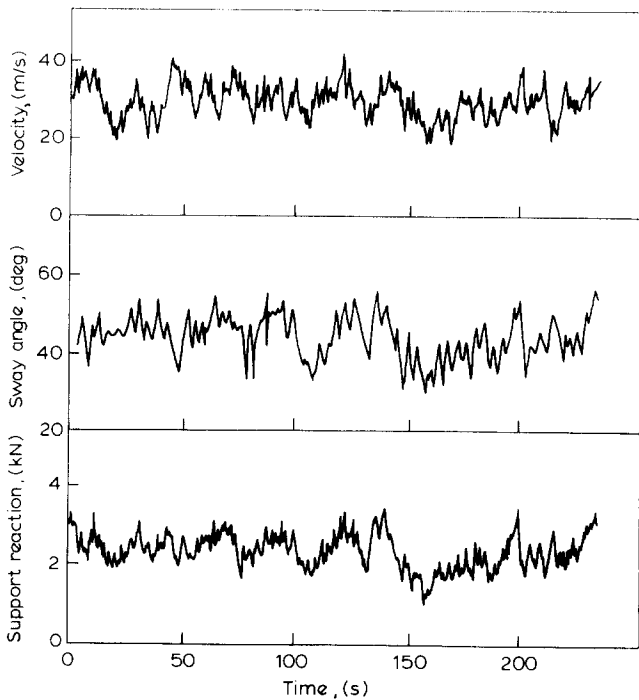


Figure 2 Typical simulated response records

Table 2 Mean and r.m.s. fluctuating responses

$\bar{u}$ (m/s)	$\bar{R}$ (kN)	$\sqrt{\bar{R}^2}$ (kN)	$\bar{\theta}$ (deg)	$\sqrt{\bar{\theta}^2}$ (deg)
10	0.261	0.0492	6.19	1.04
20	1.04	0.201	23.4	3.89
30	2.35	0.458	43.9	5.81

Differences between the two solutions increase with higher mean wind speeds, varying from 6% at  $\bar{u} = 10$  m/s, to 9% at  $\bar{u} = 30$  m/s. These differences can be explained by the contribution from fluctuations in line tension not accounted for in random vibration theory, which increases with higher mean velocity. Linearization of forces in random vibration analysis also may contribute to the underestimation of support loads.

The slope of the random vibration theory line was calculated as equal to 2.01, whereas a line drawn through the simulation model points exhibits a slope of 2.03. If dynamic behaviour of the line was ignored (e.g. a rigid bar instead of a line) then the support reaction would be directly proportional to velocity squared, i.e. the slope would be 2.00. These results appear to indicate that the exclusion of resonant dynamic response when estimating the support reaction  $R$ , may be justified.

**Spectra**

The spectrum of the support reaction is plotted in Figure 4 for  $\bar{u} = 30$  m/s, for both the simulation results and for the linearized random vibration theory.

Immediately obvious from this figure, is the close agreement between the spectra at low frequencies, and the small contribution of the resonant frequencies to the total mean square value. The latter observation is attributed to the higher aerodynamic damping at high mean wind speeds (20–25% of critical for  $\bar{u} = 30$  m/s). Small resonant peaks occur at the first sway mode and first in-plane mode, the latter appearing in the simulation model spectrum only. However, at low velocities the resonant frequencies are

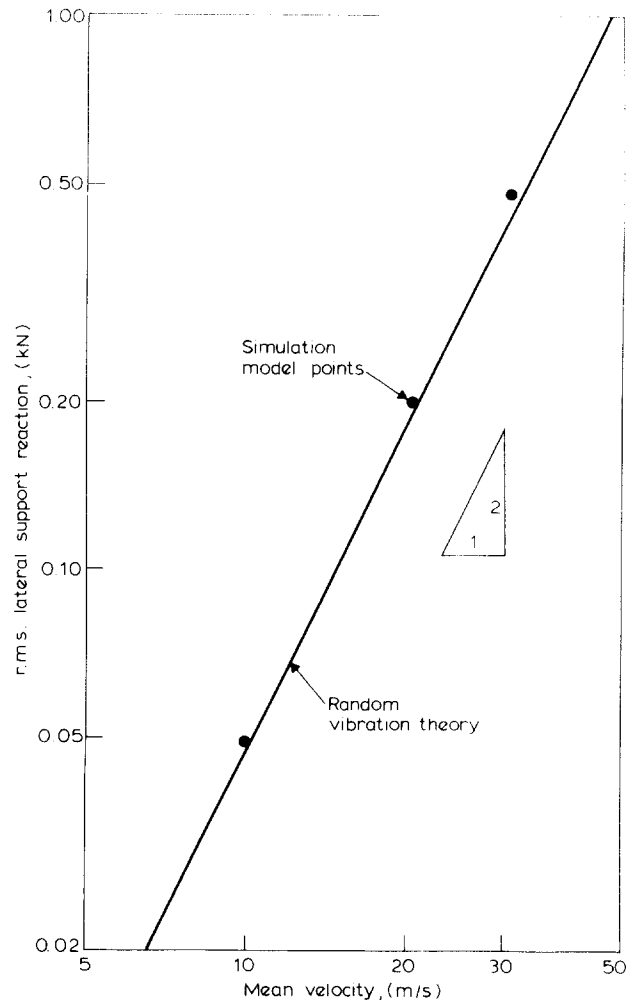


Figure 3 r.m.s. support reaction

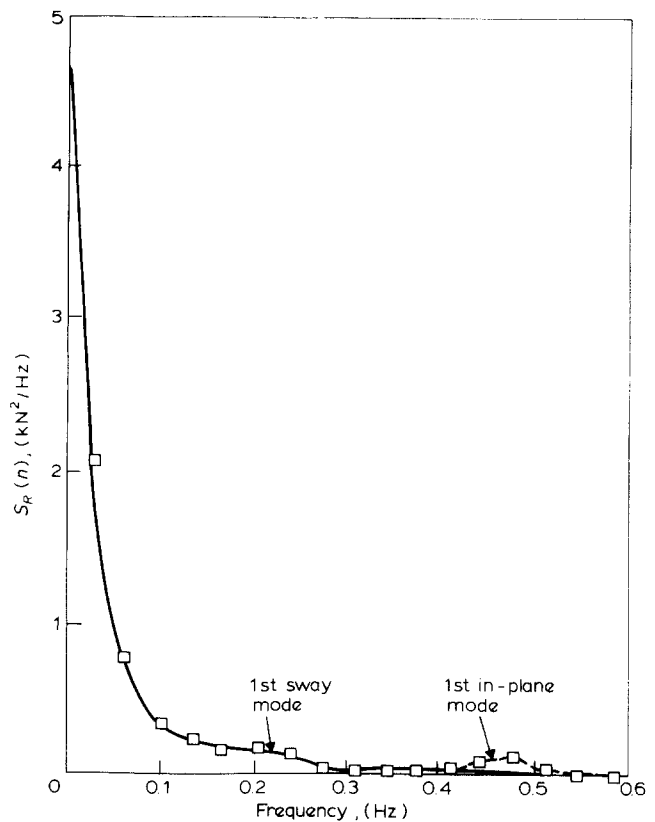


Figure 4 Spectral density of support reaction ( $\bar{u} = 30$  m/s). (—□—), simulation (nonlinear); (—), random vibration theory (linear)

more pronounced in the spectra because the aerodynamic damping drops. Although the inplane mode contribution is significant in amplitude relative to the random vibration theory value at this frequency, it is quite apparent that overall it makes little difference to the total mean square and r.m.s. values. This is also indicated in *Figure 3*.

A comparison of line deflection response between the two methods is of limited use. The use of random vibration theory to predict deflections as expounded by Manuzio and Paris<sup>3</sup> does not allow for the mean deflection of the line under wind. The latter has two effects: the moment arm of the horizontal wind loading is reduced and the moment arms of the restoring gravitational forces are increased. The two effects combine to produce reduced sway angles and lateral deflections at high wind speeds. The spectrum of sway angle from the simulation method is shown in *Figure 5*. The prominence of the first sway mode frequency can be seen in this figure.

#### Design factors

The span reduction factor  $\alpha$ , for support reaction is defined as the ratio of the maximum expected reaction,  $R$ , to the unmodified reaction calculated from the peak gust velocity, i.e.:

$$\alpha = \frac{R_{\max}}{\frac{1}{2} \rho_{\text{air}} C_d D u_{\max}^2 l / 2} \quad (21)$$

As mentioned earlier in the paper, this reduction factor accounts for the reduction in correlation of wind with distance along the line, as well as dynamic effects.

The peak velocity,  $u_{\max}$ , in the denominator is difficult to define, as it depends upon the frequency response of the instrument used to measure it, and on the duration of the record. This results in estimates of  $\alpha$  having considerable variability.

The gust factor,  $G$ , is defined as in (21), except  $\bar{u}$  is used instead of  $u_{\max}$ , and represents the ratio of peak to mean response. *Table 3* shows reduction and gust factors obtained for various velocities, where again results presented from the

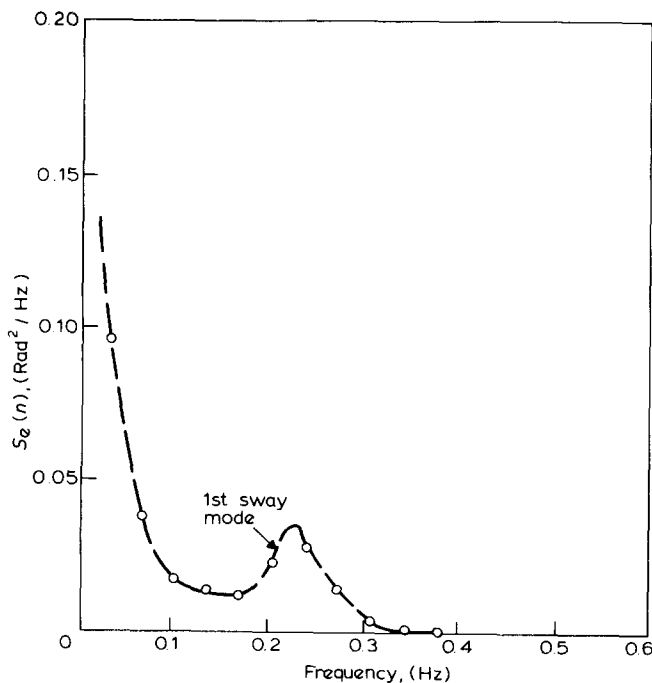


*Figure 5* Spectral density of centre-span sway angle. (—○—), simulation.  $\bar{u} = 30$  m/s

*Table 3* Span reduction and gust factors

$\bar{u}$ (m/s)	Simulation model		Random vibration theory	
	$\alpha$	G	$\alpha$	G
10	0.662	1.55	0.626	1.46
20	0.665	1.57	0.628	1.48
30	0.685	1.62	0.630	1.49

simulation model are an ensemble average of four runs.

The span reduction factors, in both cases, have been calculated using a maximum velocity  $u_{\max}$ , derived using equation (1) and the method of Davenport,<sup>13</sup> with a cut off frequency of 8.8 Hz and a time duration of 233 s. These values correspond to the values used in the simulation method. The value of  $u_{\max}/\bar{u}$  so determined was close to 1.53 for all mean wind velocities.

In all cases, the factors given by the simulation model are higher than the corresponding ones from the random vibration theory. For both solutions, the factors vary little with increases in velocity. Comparison between the two methods shows that gust factors and reduction factors differ by about 7%.

Limited tests were conducted with an intensity of turbulence of 0.30. The simulation model results gave 20–25% increase in  $G$ .

#### Conclusions

- (1) The simulation allows the nonlinear behaviour of transmission lines to be treated, and highlights the significance of in-plane modes in the response. Excitation of in-plane modes is not achieved in random vibration theory because linearizing assumptions suppress these modes.
- (2) Conventional linearized random vibration theory slightly underestimates the r.m.s. support reaction.
- (3) Results have supported the conclusions from random vibration theory that at high velocities, dynamic response is not dominant due to the high aerodynamic damping.
- (4) Conventional random vibration theory needs to be modified to consider the fluctuating behaviour about the mean deflected position, if it is to predict the line deflections accurately. The simulation method described in this paper can be used to predict deflections realistically.
- (5) Span reduction factors and gust factors are somewhat higher than those currently used in design. An increase in  $G$  of 20–25% occurs with a doubling of wind turbulent intensity.

Future developments should include the incorporation of vertical velocity components and hence vertical aerodynamic forces.

Although random vibration theory has shown itself acceptable for determining support reactions, it shows significant deficiencies when estimating line deflections. Therefore, the simulation approach could prove most useful in studying the clashing of parallel lines in strong winds.

#### Acknowledgements

The support and encouragement of Mr B. J. Bulman of the Queensland Electricity Generating Board for the work described in this paper is gratefully acknowledged by the authors.

References

- 1 Davenport, A. G. 'The response of slender line-like structures to a gusty wind', *Proc. I.C.E.* 1962, **23**, 389
- 2 Davenport, A. G. 'Gust response factors for transmission line loading', *Proc. 5th Int. Conf. Wind Eng.*, Fort Collins, July 1979
- 3 Manuzio, C. and Paris, L. 'Statistical determination of wind loading effects on overhead line conductors', *C.I.G.R.E. Rep.* 231, 1964
- 4 Castanheta, M. N. 'Dynamic behaviour of overhead power lines subject to the action of wind', *C.I.G.R.E. Rep.* 2208, 1970
- 5 Armitt, J. *et al.* 'Calculation of wind loadings on components of overhead lines', *Proc. I.E.E.* 1975, **122**, 1247
- 6 Holmes, J. D. 'Computer simulation of multiple, correlated wind records using the Inverse Fast Fourier Transform', *Civ. Eng. Trans., I.E. Aust.* 1978, **CE20**, 67
- 7 Holmes, J. D. 'Monte Carlo simulation of the wind-induced response of a cable-stayed bridge', *Proc. 3rd Int. Conf. Appl. Stat. Probability Soil Struct. Eng.* Sydney, January 1979
- 8 Davenport, A. G. 'The spectrum of horizontal gustiness near the ground in high winds', *Quart. J. Roy. Met. Soc.* 1961, **87**, 194
- 9 Roussel, P. 'Numerical solution of static and dynamic equations of cables', *Comp. Meth. Appl. Mech. Eng.* 1976, **9**, 65
- 10 Watts, A. M. 'Efficient numerical solution of the dynamic equations of cables', *Australian Appl. Math. Conf.*, Katoomba, 1979
- 11 Frith, R. J. and Watts, A. M. 'Dynamic behaviour of transmission line conductors under the influence of wind', *Ann. Eng. Conf.*, I.E. Aust, Adelaide, 1980
- 12 Irvine, H. M. and Caughey, T. K. 'The linear theory of free vibrations of a suspended cable', *Proc. Roy. Soc. A.* 1974, **341**, 299
- 13 Davenport, A. G. 'Note on the distribution of the largest value of a random function with application to gust loading', *Proc. I.C.E.* 1964, **28**, 187

Nomenclature

<i>A</i>	cross-sectional area of line
<i>c</i>	decay constant (equation (2))
<i>C<sub>d</sub></i>	drag coefficient
<i>d</i>	separation distance (equation (2))
<i>D</i>	line diameter
<i>E</i>	Young's modulus

<i>f</i>	force/unit length
<i>F</i>	dimensionless force
<i>G</i>	gust factor
<i>h</i>	dimensionless space step = $\Delta x/l$
<i>H</i>	horizontal tension in static state
<i>I<sub>u</sub></i>	longitudinal turbulence intensity
<i>j</i>	node number
<i>l</i>	span
<i>n</i>	(1) frequency, (2) number of time step
<i>N</i>	total number of time steps per record
<i>R</i>	(1) dimensionless line tension, (2) lateral component of support reaction
<i>s</i>	distance along line
<i>S(n)</i>	spectral density
<i>t</i>	time
<i>T</i>	line tension
<i>T<sub>1</sub></i>	tension in static state
<i>u</i>	velocity
<i>x</i>	position vector
<i>x</i>	} Cartesian coordinate system
<i>y</i>	
<i>z</i>	
<i>X, Y, Z</i>	
$\alpha$	span reduction factor
$\Delta\tau$	dimensionless time step
$\Delta x$	element length (in reference condition)
$\lambda_u$	peak wavelength (equation (1))
$\rho$	mass/unit length
$\rho(n)$	normalized co-spectral density (equation (2))
$\rho_{air}$	air density
$\theta$	sway angle at centre span
$\epsilon$	strain

Subscripts:

0	reference state
<i>r</i>	relative value

Superscripts:

—	mean value
'	fluctuating value